Time series analyses of forest cover change according to elevation gradient in Gansu province of China

Y. Wang, E. A. Kurbanov, O. N. Vorobiev

Center for Sustainable Forest Management and Remote Sensing, Volga State University of Technology, Yoshkar-Ola 424000, Russia
E-mail: kurbanovea@volgatech.net

This study used the time series of Landsat satellite data to define the Remote Sensing Environmental Index (RSEI) for the forests around Zhangye city in Gansu province of China from 1990 to 2021 with respect to determining forest cover changes. The elevation gradient of the estimated territory was also studied and analysed. On the basis of traditional regression method, Landsat time series were divided into three RSEI (Remote Sensing Environmental Index) curve trends: logarithmic, logistic, and exponential type, which were used to evaluate the current ecological state of the forest. Over the past 32 years, Zhangye forest area ecology has consistently improved, with 96.0 % of the forest area RSEI increasing, 1.4 % decreasing and 2.6 % remaining unchanged. The linear trend dominates the ecological changes in the forest. The RSEI findings indicate that ecology of 89.9 % of the forest areas is stable, while 10.1 % of the forest areas are unstable. There are obvious differences in RSEI trends and among diverse types of forests according to the elevation gradient. The RSEI rise area shows approximately normal distribution between 2500 and 4500 m, and the RSEI decline area forms a bimodal distribution in the two intervals of 1500–2500 and 3000–4500 m. Through the detailed differentiation of forest cover time series trends, the forest areas that need to be protected are more clearly defined.

Keywords: RSEI, time series, forest cover, monitoring, Landsat, China, trend analysis, logistic model

Accepted: 20.10.2022
DOI: 10.21046/2070-7401-2022-19-5-176-189

Introduction

Forests have a significant and indispensable role in preserving the ecological balance, enhancing the ecosystem, and sustaining the quality of the environment for people to live in (Badea, Apostol, 2020; Zhao et al., 2019). Monitoring of the forest ecosystems is crucial for providing information necessary for research of the global change and sustainable forest management. There is an increasing international trend towards the use of powerful and flexible geospatial technologies such as remote sensing in various applications (Kurbanov et al., 2020, 2022). Through the use of remote sensing, continuous spatiotemporal patterns can be observed. This aims to accomplish quantitative inversion of variables including forest canopy closure and biomass accumulation in addition to obtaining information on the quantity of forest resources, geographical distribution, and dynamic change (Gao et al., 2013; Kurbanov et al., 2007). Such a method can satisfy the demands of different levels of monitoring and analysis of forest resources and environmental processes.

Currently, the normalized difference vegetation index (NDVI) is widely used to estimate global forest cover and greenness and is considered a reliable ecological indicator of vegetation health and productivity (Eastman et al., 2013; Yu et al., 2020; Yun Chen et al., 2022). Meanwhile, in arid and semi-arid areas NDVI alone cannot fully reflect the water stress state of vegetation (Zhang et al., 2022). Recently, the ecological complexity index combining several vegetation indicators on the basis of NDVI (Mora, 2022), the remote sensing-based ecological index (RSEI) (Lai et al, 2022; Mu et al., 2022), and other comprehensive parameters showed more suitable results for forest ecological research in arid and semi-arid regions.

Trend analysis is a common method used for remotely sensed forest change monitoring, where the slope value of the trend line accurately represents the vegetation change average annual rate during the estimated period (Verbesselt et al., 2010). The slope value, often used for forest disturbance monitoring, can accurately represent the annual average change rate of vegetation during a study

period (Wessels et al., 2012). The time series trajectory fitting approach based on trend analysis assumes that a disturbance event occurs in the vegetation during the study area and uses its time as the midpoint of the entire time series trajectory (Kennedy et al., 2007). The midpoint of the trajectory is used as a curve extension to create a mathematical model for modelling vegetation change over time. Hyperbolic (Lawrence, Ripple, 1999), cubic polynomial (Jamali et al., 2014), exponential (Kennedy et al., 2007), logarithmic (Riano et al., 2002), logistic model (Qiu et al., 2017), and multi-exponential combinations of mathematical models (Wang et al., 2019) have been used to monitor forest disturbance restoration and forest ecological change research. However, vegetation may experience different short-term changes in a long-term time series, which may go undetected or completely masked in trend analysis (De Jong et al., 2012; Jamali et al., 2014).

The main objective of the study was to analyse changes occurring in forests near Zhangye city of Gansu province of China over the past 32 years. To achieve this objective, the following tasks were accomplished:

- Extraction of the Zhangye forest region from the Landsat images and calculation of the year-by-year RSEI for the forest region over a 32-year period.
- Three time-series curve trends based on the RSEI model of logarithmic, logistic, and exponential types were constructed and analyzed.
- Analysis of the relationship between different forest ecological types and their altitudes.

Research area

Zhangye city of the Gansu Province of the People's Republic of China is located in the middle of Hexi (Gansu) corridor, in the middle and upper reaches of China's second largest inland river basin (*Fig. 1*).

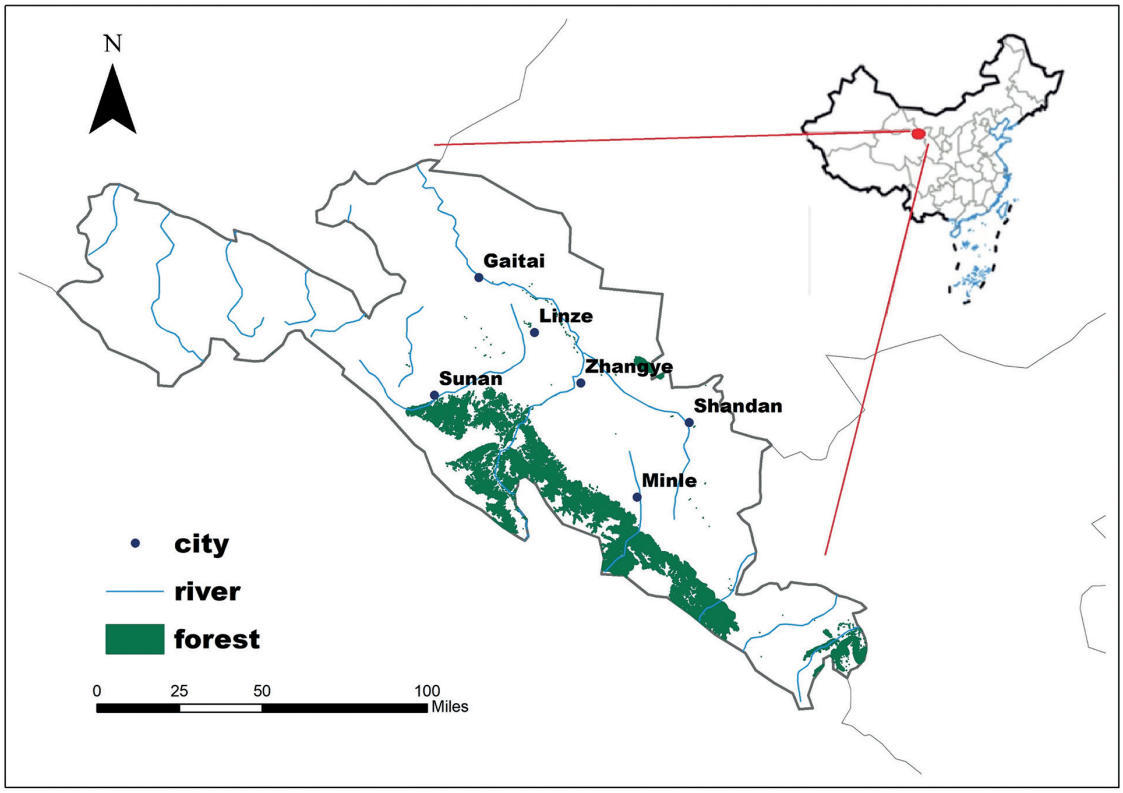

Fig. 1. Location of forest area in Zhangye

East longitude is 97° 20′–102° 12′, north latitude is 37°28′–39° 57′, with a total area of 38,600 km^2. The majority of locations have a typical temperate arid climate with low precipitation and high evapo-

ration (Peng et al., 2007). The Qilian Mountains area has a mountain climate with more precipitation and lower temperatures than in the surrounding area. The distribution of precipitation in the region is uneven. The average annual precipitation is 112–354 mm, and the annual average temperature is 4.1–8.3 °C. The urban area is in the centre, covering 3,661 km^2, which makes approximately 9.5 % the total area; in the southwest there are the Qilian Mountains, and in the northeast local flat oases and deserts. The annual precipitation in the Qilian Mountains is between 300 and 500 mm, and there is water run-off from melting glaciers and seasonal snow covers. The forests are mainly located in the Qilian Mountains, with an average annual temperature of –0.6 to 2 °C, recharged by snow and ice melt water, and they are runoff forming areas. The forests consist of shrub and plantation forests, the main tree types being Qinghai spruce (*Picea crassifolia*), desert poplar (*Populus euphratica*), jujube (*Ziziphus jujube*), red willow (*Salix laevigata*), and haloxylon (*Haloxylon ammodendron*) (Chang et al., 2014; Xiao, Huang, 2016).

Data and methods

Determination of the RSEI time series

The remote sensing images required for the experiment come from the Landsat image data provided by Unites States Geological Survey (USGS) in the Google Earth Engine (GEE) platform (Gorelick et al., 2017). Images from Landsat-5 (1990–2011), Landsat-7 (2012), and Landsat-8 (2013–2021) were used in the study. The time acquisition of the images has been chosen from June to October, when the forest is at its most luxuriant vegetation period. Cloud removal and image stitching were processed on the GEE platform. For classification in the GEE platform, the 32-year forest cover area in the region was extracted in 1990, 2005 and 2021. The RSEI was calculated (Xu et al., 2018) according to the formula:

$$\mathrm{RSEI} = f(\mathrm{Greenness}, \mathrm{Wetness}, \mathrm{Dryness}, \mathrm{Heat}).$$

Greenness is represented by NDVI. Wetness is the humidity component calculated for the Tasseled Cap transformation (Jin, Sader, 2005). Dryness uses normalized difference impervious surface index (NDSI), which is based on the combination of the index-based built-up index (IBI) and soil index (SI) (Xiong et al., 2021). Heat is the land surface temperature (LST). In order to eliminate the influence of periodicity and irregular fluctuations of time series and highlight the overall development trend of time series, we smoothed the 32-year original RSEI time series with the Savitzky–Golay filter in GEE.

When the growth of vegetation is disturbed by external events, the vegetation will quickly enter a state of rapid improvement or deterioration in a certain year (Wang et al., 2022). This moment corresponds to the position where the maximum slope appears on the profile of the forest RSEI time series curve (Qiu et al., 2017). The largest absolute value of the first derivative in the time series curve is the maximum change moment in this curve (Wang et al., 2019). Based on this we calculated the maximum year change of the RSEI in each image area.

Extension of the time series curve according to the determined time

To ensure more accurate fits, the time series curves were extended using the RSEI maximum change year as the midpoint. The maximum value t of the absolute value of the first derivative calculated in the pixel area is taken as the midpoint of the extended time series curve. The time series length of this study is 32, and the time series midpoint position is 16. The extended timing length L can be obtained by formula:

$$L = \begin{cases} 32 & if\ t = 16, \\ 2(32 - p) & if\ t < 16, \\ 2(p - 1) & if\ t > 16. \end{cases}$$

Determination of linear and nonlinear trends

We assume that when forest cover changes, whether it improves or declines, it will tend to move from one stable state to another. Logistic function fitting of the extended RSEI curve was used to distinguish whether the forest time series in the region was a linear change or a curve change (Wang et al., 2019). In MATLAB software, the time series for each pixel of Landsat imagery was fitted with a four-parameter logistic function:

$$f(t) = \frac{a}{1 + e^{b(t-c)}} + d,$$

where a is the variation of RSEI in 32 years; b is the slope of the RSEI time series curve at time t; c is the location where the fitting value is equal to $(a + b)/2$, and d is the RSEI value of the initial year. The ordinary least squares method was used to obtain the values of the four parameters. The joint hypotheses test method was used to test the function fit, and t significance values less than 90 % were categorised as linear trends. Logarithmic type, logistic type, and exponential type will be further distinguished for the parts with significance greater than or equal to 90 %.

According to the logistic function vegetation fitting research, the turning point on the logistic function S-shaped curve, which is also the fastest changing location in curve curvature, represents vegetation change year (Zhang et al., 2003). The formula for the curve curvature K is

$$K = b^3 cz \left\{ \frac{3z(1-z)\cdot(1+z)^3\left[2(1+z)^3 + b^2c^2z\right]}{\left[(1+z)^4 + (bcz)^2\right]^{5/2}} - \frac{(1+z)^2(1+2z-5z^2)}{\left[(1+z)^4 + (bcz)^2\right]^{3/2}} \right\},$$

where $z = e^{a+bt}$; a, b, c are the parameters. The first derivative of K is the maximum or minimum value in the curvature change rate. If $b < 0$, the time point corresponding to the two maximum values in the curvature change rate is the turning point, and it is determined that the pixel area conforms to the logistic curve. If $b > 0$, the moment corresponding to the two minima in the rate of curvature change is the turning point. Finally, the curve types are further classified according to the distribution number of the maximum or minimum values during the study time period. In the 1990–2021 period, if there are two maximum or minimum values, the pixel area conforms to the logistic curve. When only one maximum or minimum value is distributed in the study period, the year in which the maximum value is greater than c, the pixel area conforms to the logarithm mode, otherwise it is the exponential mode.

Classified altitude statistics

In ArcGIS Pro package, the area of 9 forest types was extracted, with a total of 3 361 334 points, and the DEM (Digital Elevation Model) data was combined to obtain the elevation information of each type. In SPSS Statistics 23, the point data of different forest types were counted, and the difference in elevation of different forest types was calculated. The F-test and T-test determines whether the variances of the two populations are significantly different. If the variances of the two populations are not significantly different, an assumed equal variance is used; if the variances of the two populations are significantly different, they are not assumed equal (Yang et al., 2004).

Results and discussion

Extraction of Zhangye forest area RSEI values according to 32 years Landsat imagery showed that 96.0 % of the study area RSEI increased, 1.4 % decreased and 2.6 % remained the same. Based on this, a pixel-by-pixel curve was fitted to the RSEI images over the 32-year period. Nine different forest areas of stable, logarithmic rise, logarithmic fall, logistic rise, logistic fall, exponential rise, exponential fall, linear rise, and linear fall were obtained. The statistics for this area are shown in *Table 1*. Compared to a purely linear trend, it can be seen that the division of growth and decline regions is finer. In the past 32 years, most of the RSEI values in forest areas have been in the rising part, followed

by the constant part, and finally the falling part. From a spatial point of view, the constant area and the falling area are located at the outermost periphery of the forest area, and the central area is the growth area.

Table 1. The 9 different types of forest change area

Type	Curve	Area, km^2
Stable		86.85
Logarithm rise		35.19
Logarithm fall		0.04
Logistic rise		38.53
Logistic fall		0.56
Exponential rise		5.17
Exponential fall		0.64
Linear rise		1998
Linear fall		29.1

In the rise area, the linear change is evenly distributed, the logarithmic is mostly distributed at the edge of the growth area, the logistic is distributed in the center of the rise area, and the exponential rise area is commonly in the vicinity of the logistic growth (*Fig. 2*). In the fall area, the forest is fragmented and located at the periphery away from the forest centre.

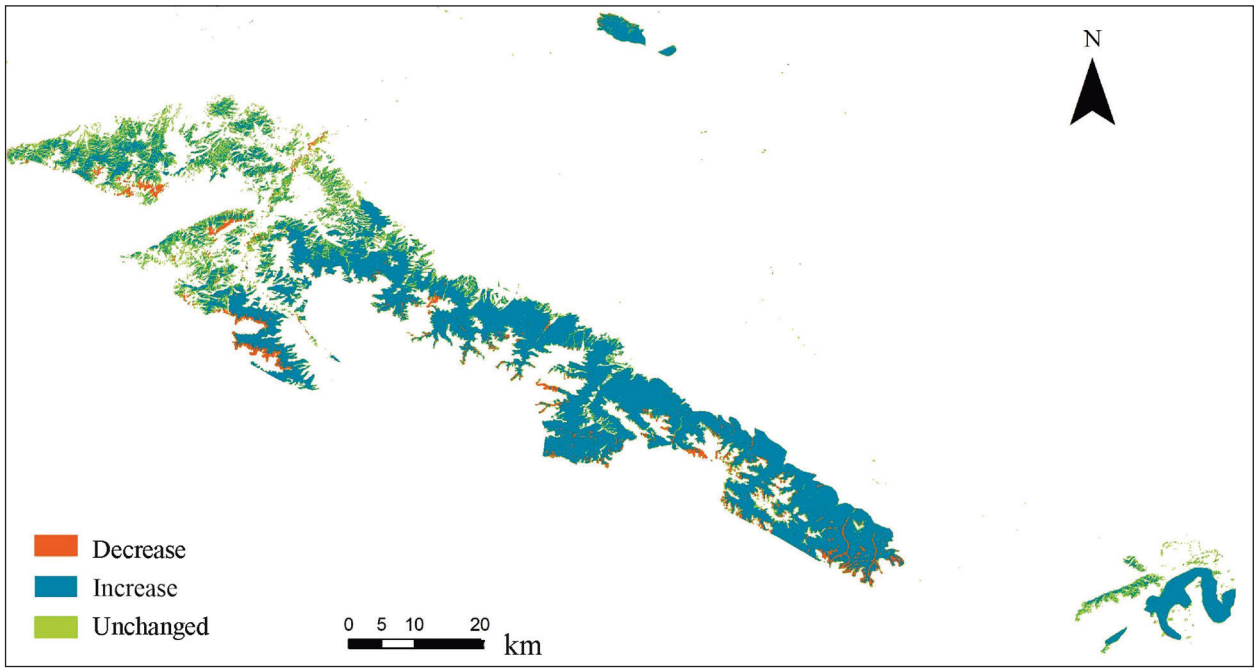

a

Fig. 2a. Forest maps of Zhangye: forest change map

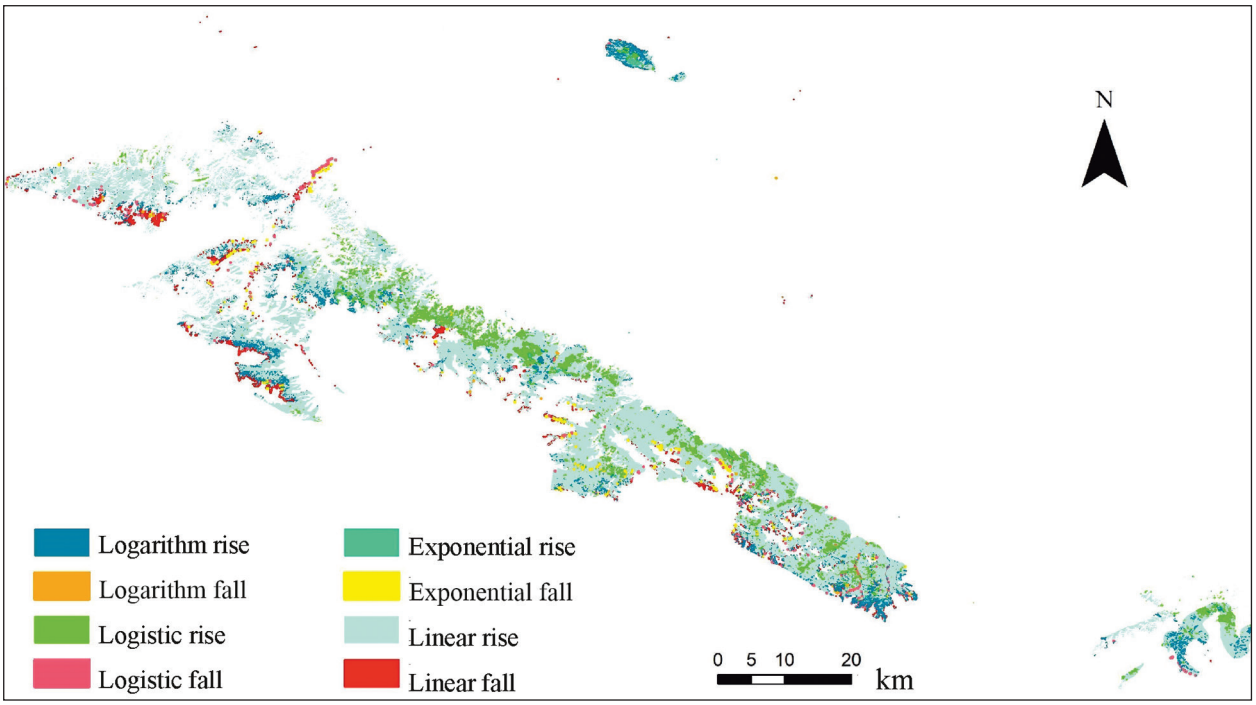

b

Fig. 2b. Forest maps of Zhangye: time series fitting distribution map of forest area combined with various curves

Based on the current forest ecological stability in the research area, the forest is divided into stable and unstable areas. Continuously stable, logarithmic rise, logistic rise, logarithmic fall, logistic fall are all considered stable areas. Linear rise, linear fall, exponential rise, and exponential fall are considered unstable areas. Logarithm and logistic both illustrate the transition from change to stability. The exponential function represents the transition from stability to change. According to the statistics, the change area accounts for 89.9 %, while the stable area accounts for 10.1 % (*Fig. 3a*, see p. 182). In the stable area, continuous stability accounted for 57.7 %, logarithm increased for 20.3 %, logarithm decreased for 0.03 %, logistic increased for 21.6 %, and logistic decreased for 0.35 %. In the change area, the ecological growth area accounted for 98.5 %, and the ecological reduction area accounted for 1.5 %. In the growth area, linear growth accounted for 95.9 %, an increase to stable 3.8 %, and stable to increase 0.3 % (see *Fig. 3*). In the fall area, linear reduction accounts for 95.4 %, reduced to stable 2.3 %, and stable to reduced 2.3 %.

Statistics for the nine forest types and their respective altitudes are shown in *Table 2* to further investigate how these factors affect different forest types.

Table 2. Forest change types corresponding elevation statistics

Change type	Count	Average	Median	95 % confidence interval		Min	Max
				Lower Bound	Upper Bound		
Stable	166 304	3212	3198	3210	3215	1356	4606
Logarithmic rise	58 614	3363	3398	3360	3366	1921	4305
Logarithmic fall	73	3419	3672	3280	3556	1782	4115
Logistic rise	62 189	3090	3099	3087	3092	1372	4149
Logistic fall	1021	3285	3528	3242	3328	1693	4152
Exponential rise	8034	3304	3324	3299	3309	1698	4100
Exponential fall	1087	3485	3664	3448	3521	1716	4256
Linear rise	3019	3218	3222	3218	3218	1356	4585
Linear fall	45 315	3728	3805	3724	3731	1376	4551

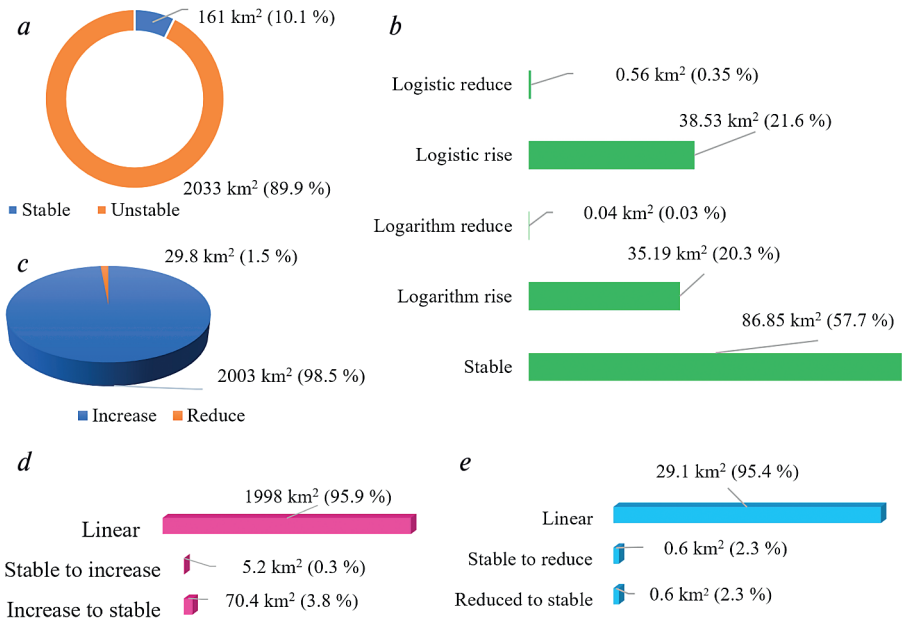

Fig. 3. Distribution of Zhangye forests according to: *a* — stable and unstable areas; *b* — stable area; *c* — unstable area; *d* — growth area; *e* — reduction area

The lowest point in the forest area is 1356 m above the sea level, and the highest point is 4606 m. Most of these forest ecosystems are concentrated in mountainous areas between 3200 and 3800 m. From the average elevation, the increased part is lower, and the decreased part is higher (*Fig. 4*, see p. 183). From the perspective of altitude, distribution of the increasing part tends to be more normal between 2500 and 4500 m, and the decreasing part forms two trends in the two intervals of 1500–2500 and 3000–4500 m.

Three different types of forest with trends in elevation data have been compared: logistic, logarithmic, and exponential. According to the results shown in *Table 3*, the data are significantly different, the homogeneity test significant values are less than 0.001, and the data are independent of each other. When comparing the same type of forest growth areas with the decline areas in *Table 4*, the homogeneity test significant values are less than 0.001, and their elevation distribution is also significantly different.

Table 3. Trends of 3 curves and separation of data

Trend of curves		Levine variance equality		Mean equivalence	
		F-test	*p*-value	T-test	*p*-value
Logarithmic rise	Assume equal variances	1477	<0.001	103.6	<0.001
	Equal variances not assumed			94.1	
Logistic rise	Assume equal variances	2475	<0.001	–94.8	
	Equal variances not assumed			–106.6	
Exponential rise	Assume equal variances	2520	<0.001	23.0	
	Equal variances not assumed			34.9	
Logarithmic fall	Assume equal variances	67	<0.001	–7.3	
	Equal variances not assumed			–4.47	
Logistic fall	Assume equal variances	1195	<0.001	–37.6	
	Equal variances not assumed			–20.2	
Exponential fall	Assume equal variances	642	<0.001	–21.5	
	Equal variances not assumed			–13.1	

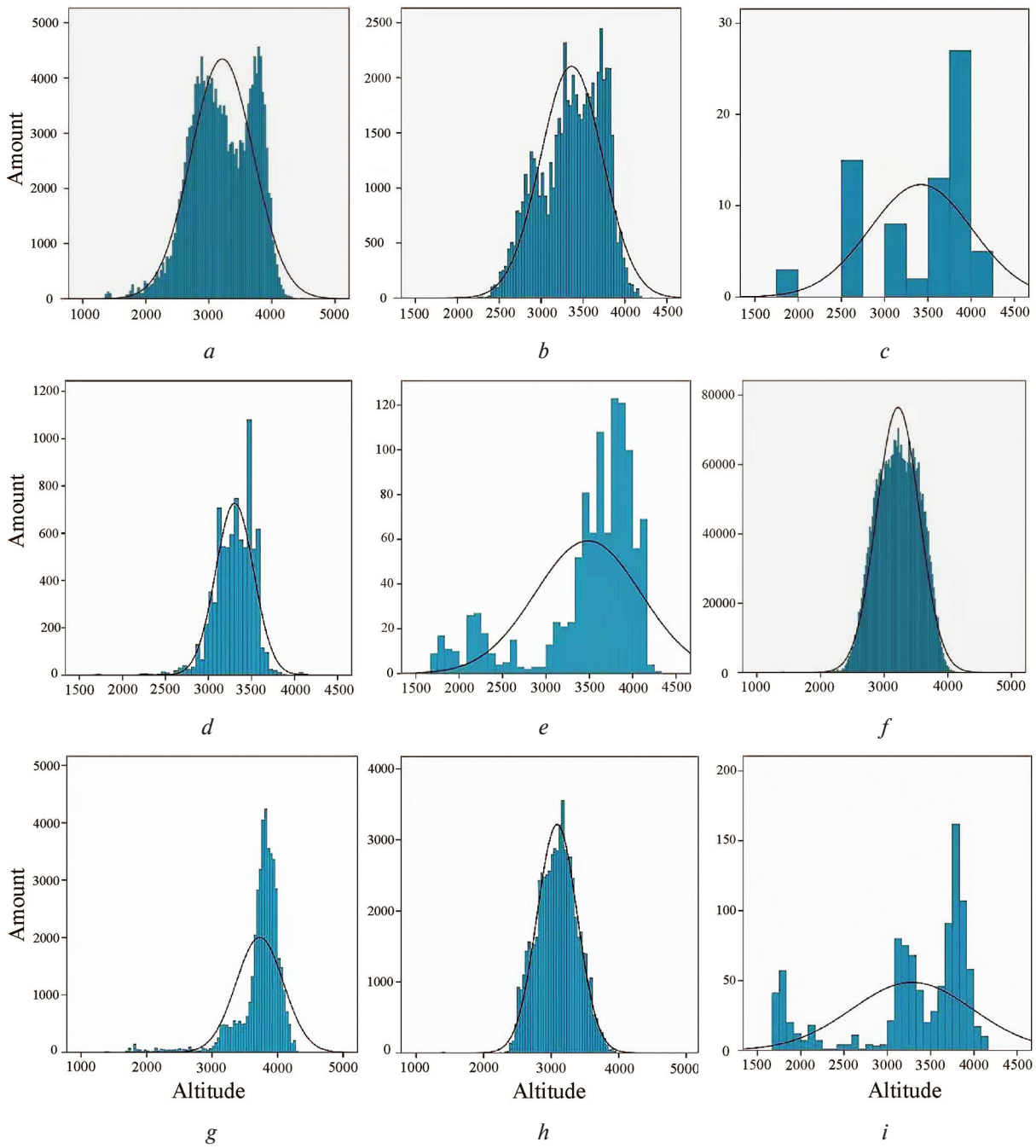

Fig. 4. Different fitting curves correspond to the altitude distribution: *a* — Stable forest altitude statistics; *b* — Logarithmic rise forest altitude statistics; *c* — Logarithmic fall forest altitude statistics; *d* — Logistic rise forest altitude statistics; *e* — Logistic fall forest altitude statistics; *f* — Exponential rise forest altitude statistics; *g* — Exponential fall forest altitude statistics; *h* — Linear rise forest altitude statistics; *i* — Linear fall forest altitude statistics

The 32-year forest ecological trend in this study area has improved, and the area of forest ecological stability is significantly larger than the area of ecological degradation. The areas with declining ecosystems are mostly in the periphery of the forest region, showing that the overall forest area is in a healthy growth stage and only fluctuates in the marginal parts. By fitting a 32-year trend to each pixel, it is possible to further delineate the original growth areas and better determine the degree of stability within them. According to the experiment, the Zhangye forest in most study areas is still changing. The vast majority of the change area is taken up by the ecological increase. The linear trend still occupies the largest part in the rise and the decrease areas. In the stable zone, most of the areas belong to the current high and continuous ecological quality state.

Table 4. The 3 curve area data separation of ecological rise and ecological fall

Trend of curves		Levine variance equality		Mean equivalence	
		F-test	*p*-value	T-test	*p*-value
Logarithmic	Assume equal variances	61	<0.01	−1.3	<0.01
	Equal variances not assumed			− 0.8	
Logistic	Assume equal variances	2757	<0.01	−20.1	
	Equal variances not assumed			−8.9	
Exponential	Assume equal variances	2002	<0.01	−18.9	
	Equal variances not assumed			−9.7	
Linear	Assume equal variances	2965	<0.01	−321.0	
	Equal variances not assumed			−298.8	

Due to the strong ecological sensitivity of the Hexi corridor area where Zhangye is located, the sustainability of its forests is easily affected by natural factors such as climate (Wang, 2021). At the same time, human activities also have a significant impact on forest ecology. The exponential type area extracted in this experiment indicates that the forest RSEI value in this area has changed from a stable period to a rapidly changing period in recent years, and it is the area that requires attention in terms of ecological protection. Logarithmic-type and logistic-type areas indicate that the current forest condition is stable, and the analysis of the change period can provide an in-depth perspective on the reasons for forest ecological changes.

From the elevation information of the studied areas, it can be seen that there are differences in the altitudes of different forest types. The high-altitude area has a weakening trend in stability compared with the low-altitude areas. Trend variance between different forest types shows that altitude is one of the important factors of their ecological changes (Tian et al., 2021). The different altitudes in the mountainous region significantly affect the climate and forest ecology of the region, which is in line with the conclusion of this experiment. Compared with spatial location, altitude has a more significant impact on forest sustainability, and the influence of human factors may be one of the reasons for disturbance impact in forest areas borders.

Due to the limitations of the curve-fitting method in this study, the models cannot be accurately fitted as a function of RSEI of repeatedly fluctuating forest areas. For the case of RSEI time-series repeatedly changing due to multiple change events during the study time period, we only categorized them as linear trends based on the overall trend. If this could be extracted to match a more suitable curve model for future studies, it would more accurately assess the processes of forest ecological quality change.

Conclusions

This experiment is based on the method of pixel-by-pixel trend fitting of the RSEI values in the forest area of Zhangye for 32 years. Overall, the forested regions in Zhangye are in a healthy ecological state, with the majority of them experiencing ecological increase or positive ecological stability. Among them, the linear trend accounts for most of the estimated change trends. The main ecological changes were identified near the forest area boundaries, with the central areas keeping a high level of ecological status. According to the altitude analysis, there is significant heterogeneity in the different forest trend types, and the increasing areas tend to be normally distributed, while the decreasing areas display a bimodality trend. Multiple change trend fitting and change time extraction in forest areas could be beneficial for forest ecology research in the future.

The reported study was funded by Russian Foundation for Basic Research (grant number 19-55-80010/21), Ministry of Science and Technology (MOST) (grant number 2018YFE0184300), and National Research Foundation (NRF) (grant number 120456) according to the research project No. 19-55-80010; CSC (China Scholarship Council) No. 202110280009.

References

1. Badea O., Apostol E., Forest science innovation for sustainable forest management, improvement of human welfare, and quality of life under global environmental changes, *Science of The Total Environment*, 2020, Vol. 701, Art. No. 134429, 4 p., https://doi.org/10.1016/j.scitotenv.2019.134429.
2. Chang X., Zhao W., Liu H., Wei X., Liu B., He Z., Qinghai spruce (*Picea crassifolia*) forest transpiration and canopy conductance in the upper Heihe River Basin of arid northwestern China, *Agricultural and Forest Meteorology*, 2014, Vol. 198–199, pp. 209–220, http://dx.doi.org/10.1016/j.agrformet.2014.08.015.
3. De Jong R., Verbesselt J., Schaepman M. E., de Bruin S., Trend changes in global greening and browning: contribution of short-term trends to longer-term change, *Global Change Biology*, 2012, Vol. 18, No. 2, pp. 642–655, https://doi.org/10.1111/j.1365-2486.2011.02578.x.
4. Eastman J. R., Sangermano F., Machado E. A., Rogan J., Anyamba A., Global trends in seasonality of Normalized Difference Vegetation Index (NDVI), 1982–2011, *Remote Sensing*, 2013, Vol. 5, No. 10, pp. 4799–4818, https://doi.org/10.3390/rs5104799.
5. Gao G., Xin Z., Ding G., Li C., Zhang J., Linag W., An Y., He Y., Xiao M., Li W., Forest health studies based on remote sensing: a review, *Acta Ecologica Sinica*, 2013, Vol. 33, No. 6, pp. 1675–1689, https://doi.org/10.5846/stxb201112011838.
6. Gorelick N., Hancher M., Dixon M., Ilyushchenko S., Thau D., Moore R., Google Earth Engine: Planetary-scale geospatial analysis for everyone, *Remote Sensing of Environment*, 2017, Vol. 202, pp. 18–27, https://doi.org/10.1016/j.rse.2017.06.031.
7. Jamali S., Seaquist J., Eklundh L., Ardo J., Automated mapping of vegetation trends with polynomials using NDVI imagery over the Sahel, *Remote Sensing of Environment*, 2014, Vol. 141, pp. 79–89, https://doi.org/10.1016/j.rse.2013.10.019.
8. Jin S., Sader S., Comparison of time series tasseled cap wetness and the normalized difference moisture index in detecting forest disturbances, *Remote Sensing of Environment*, 2005, Vol. 94, No. 3, pp. 364–372, https://doi.org/10.1016/j.rse.2004.10.012.
9. Kennedy R., Cohen W., Schroeder T., Trajectory-based change detection for automated characterization of forest disturbance dynamics, *Remote Sensing of Environment*, 2007, Vol. 110, No. 3, pp. 370–386, https://doi.org/10.1016/j.rse.2007.03.010.
10. Kurbanov E., Vorobiev O., Gubayev A., Moshkina L., Leznin S., Carbon sequestration after pine afforestation on marginal lands in the Povolgie region of Russia: A case study of the potential for a Joint Implementation activity, *Scandinavian J. Forest Research*, 2007, Vol. 22, No. 6, pp. 488–499, https://doi.org/10.1080/02827580701803080.
11. Kurbanov E., Vorobiev O., Sha J., Li X., Gitas I., Minakou C., Gabdelkhakov A., Martynova M., A survey on the use of GIS and remote sensing for sustainable forestry and ecology in Russia and China, *Current problems in remote sensing of the Earth from space*, 2020, Vol. 17, No. 5, pp. 9–20, DOI: 10.21046/2070-7401-2020-17-5-9-20.
12. Kurbanov E., Vorobev O., Lezhnin S., Sha J., Wang J., Li X., Cole J., Dergunov D., Wang Y., Remote sensing of forest burnt area, burn severity, and post-fire recovery: a review, *Remote Sensing*, 2022, Vol. 14, No. 19, Art. No. 4714, https://doi.org/10.3390/rs14194714.
13. Lai S., El-Adawy A., Sha J., Li X., Wang J., Kurbanov E., Lin Q., Towards an integrated systematic approach for ecological maintenance: case studies from China and Russia, *Ecological Indicators*, 2022, Vol. 140, Art. No. 108982, 19 p., https://doi.org/10.1016/j.ecolind.2022.108982.
14. Lawrence R., Ripple W. J., Calculating change curves for multitemporal satellite imagery: Mount St. Helens 1980–1995, *Remote Sensing of Environment*, 1999, Vol. 67, No. 3, pp. 309–319, https://doi.org/10.1016/S0034-4257(98)00092-3.
15. Mora F., A suite of ecological indicators for evaluating the integrity of structural eco-complexity in Mexican forests, *Ecological Complexity*, 2022, Vol. 50, Art. No. 101001, 19 p., https://doi.org/10.1016/j.ecocom.2022.101001.
16. Mu H., Li X., Ma H., Du X., Huang J., Su W., Yu Z., Xu C., Liu H., Yin D., Li B., Evaluation of the policy-driven ecological network in the Three-North Shelterbelt region of China, *Landscape and Urban Planning*, 2022, Vol. 218, Art. No. 104305, 11 p., https://doi.org/10.1016/j.landurbplan.2021.104305.
17. Peng H., Cheng G., Xu Z., Yin Y., Xu W., Social, economic, and ecological impacts of the "Grain for Green" project in China: A preliminary case in Zhangye, Northwest China, *J. Environmental Management*, 2007, Vol. 85, No. 3, pp. 774–784, https://doi.org/10.1016/j.jenvman.2006.09.015.
18. Qiu B., Chen G., Tang Z., Lu D. Wang Z., Chen C., Assessing the Three-North Shelter Forest Program in China by a novel framework for characterizing vegetation changes, *ISPRS J. Photogrammetry and Remote Sensing*, 2017, Vol. 133, pp. 75–88, https://doi.org/10.1016/j.isprsjprs.2017.10.003.
19. Riano D., Chuvieco E., Ustin S., Zomer R., Dennison P., Roberts D., Salas J., Assessment of vegetation regeneration after fire through multitemporal analysis of AVIRIS images in the Santa Monica

Mountains, *Remote Sensing of Environment*, 2002, Vol. 79, No. 1, pp. 60–71, https://doi.org/10.1016/S0034-4257(01)00239-5.
20. Tian A., Wang Y., Webb A. A., Liu Z., Ma J., Yu P., Wang X., Water yield variation with elevation, tree age and density of larch plantation in the Liupan Mountains of the Loess Plateau and its forest management implications, *Science of The Total Environment*, 2021, Vol. 752, Art. No. 141752, 13 p., https://doi.org/10.1016/j.scitotenv.2020.141752.
21. Verbesselt J., Hyndman R., Newnham G., Culvenor D., Detecting trend and seasonal changes in satellite image time series, *Remote Sensing of Environment*, 2010, Vol. 114, No. 1, pp. 106–115, https://doi.org/10.1016/j.rse.2009.08.014.
22. Wang C., Wang A., Guo D., Li H., Zang S., Off-peak NDVI correction to reconstruct Landsat time series for post-fire recovery in high-latitude forests, *Intern. J. Applied Earth Observation and Geoinformation*, 2022, Vol. 107, Art. No. 102704, 14 p., https://doi.org/10.1016/j.jag.2022.102704.
23. Wang J., Xie Y., Wang X., Dong J., Bie Q., Detecting patterns of vegetation gradual changes (2001–2017) in Shiyang river basin, based on a novel framework, *Remote Sensing*, 2019, Vol. 11, No. 21, Art. No. 2475, 24 p., https://doi.org/10.3390/rs11212475.
24. Wang Y., Forest ecological monitoring of the Shiyang river basin based on Google Earth Engine, *IOP Conf. Ser.: Earth and Environment Science*, 2021, Vol. 932, No. 1, Art. No. 012011, 9 p., https://doi.org/10.1088/1755-1315/932/1/012011.
25. Wessels K. J., van den Bergh F., Scholes R. J., Limits to detectability of land degradation by trend analysis of vegetation index data, *Remote Sensing of Environment*, 2012, Vol. 125, pp. 10–22, https://doi.org/10.1016/j.rse.2012.06.022.
26. Xiao Q., Huang M., Fine root distributions of shelterbelt trees and their water sources in an oasis of arid northwestern China, *J. Arid Environments*, 2016, Vol. 130, pp. 30–39, https://doi.org/10.1016/j.jaridenv.2016.03.004.
27. Xiong Y., Xu W., Lu N., Huang S., Wu C., Wang L., Dai F., Kou W., Assessment of spatial-temporal changes of ecological environment quality based on RSEI and GEE: A case study in Erhai Lake Basin, Yunnan province, China, *Ecological Indicators*, 2021, Vol. 125, Art. No. 107518, 10 p., https://doi.org/10.1016/j.ecolind.2021.107518.
28. Xu H., Wang M., Shi T., Guan H., Fang C., Lin Z., Prediction of ecological effects of potential population and impervious surface increases using a remote sensing based ecological index (RSEI), *Ecological Indicators*, 2018, Vol. 93, pp. 730–740, https://doi.org/10.1016/j.ecolind.2018.05.055.
29. Yang Y., Monserud R. A., Huang S., An evaluation of diagnostic tests and their roles in validating forest biometric models, *Canadian J. Forest Research*, 2004, Vol. 34, No. 3, pp. 619–629, https://doi.org/10.1139/x03-230.
30. Yu J., Li F., Wang Y., Lin Y., Peng Z., Cheng K., Spatiotemporal evolution of tropical forest degradation and its impact on ecological sensitivity: A case study in Jinghong, Xishuangbanna, China, *Science of The Total Environment*, 2020, Vol. 727, Art. No. 138678, 13 p., https://doi.org/10.1016/j.scitotenv.2020.138678.
31. Yun Chen Y., Wang J., Kurbanov E., Thomas A., Sha J., Jiao Y., Zhou J., Ecological security assessment at different spatial scales in central Yunnan Province, China, *PLoS ONE*, 2022, Vol. 17, No. 6., Art. No. e0270267, 19 p., https://doi.org/10.1371/journal.pone.0270267.
32. Zhang X., Friedl M. A., Schaaf C. B., Strahler A. H., Hodges J. C.F., Gao F., Reed B. C., Huete A., Monitoring vegetation phenology using MODIS, *Remote Sensing of Environment*, 2003, Vol. 84, No. 3, pp. 471–475, https://doi.org/10.1016/S0034-4257(02)00135-9.
33. Zhang X., Liu K., Li X. Wang S., Wang J., Vulnerability assessment and its driving forces in terms of NDVI and GPP over the Loess Plateau, China, *Physics and Chemistry of the Earth*, 2022, Vol. 125, Art. No. 103106, 12 p., https://doi.org/10.1016/j.pce.2022.103106.
34. Zhao J., Ma J., Zhu Y., Evaluating impacts of climate change on net ecosystem productivity (NEP) of global different forest types based on an individual tree-based model FORCCHN and remote sensing, *Global and Planetary Change*, 2019, Vol. 182, Art. No. 103010, 10 p., https://doi.org/10.1016/j.gloplacha.2019.103010.

Анализ временных рядов динамики лесного покрова по градиенту высот в провинции Ганьсу, Китай

И. Ван, Э. А. Курбанов, О. Н. Воробьёв

Центр устойчивого управления и дистанционного мониторинга лесов,
Поволжский государственный технологический университет
Йошкар-Ола, *424000*, *Россия*
E-mail: kurbanovea@volgatech.net

В исследовании для оценки динамики лесного покрова с 1990 по 2021 г. вокруг г. Чжанъе в китайской провинции Ганьсу использовались временные ряды спутниковых данных Landsat и экологический индекс дистанционного зондирования (RSEI — *англ*. Remote Sensing Environmental Index). Также был изучен и проанализирован градиент высот исследуемой территории. На основе традиционного метода регрессии временные ряды были разделены на три тренда кривых RSEI: логарифмического, логистического и экспоненциального типа, которые использовались для оценки текущего состояния леса. Результаты показали, что за последние 32 года на 96,0 % площади лесов Чжанъе показатель RSEI увеличился, на 1,4 % — понизился и остался неизменным на 2,56 %. Среди девяти графиков состояния лесного покрова преобладает линейный тренд. На 89,9 % площади лесная экосистема остаётся стабильной, на 10,1 % находится в процессе изменений. Существуют очевидные различия между типами лесов и их RSEI-трендами по градиенту высот. Увеличение RSEI наблюдается при нормальном распределении между 2500 и 4500 м, в то же время область снижения RSEI образует бимодальное распределение в двух интервалах высот: 500–2500 и 3000–4500 м. Детальная дифференциация трендов временных рядов лесного покрова позволяет более чётко определить лесные площади, которые требуют защиты.

Исследование выполнено при финансовой поддержке Российского фонда фундаментальных исследований (проект № 19-55-80010/21), Министерства по науке и технологиям (*англ*. Ministry of Science and Technology — MOST) (проект № 2018YFE0184300) и Национального исследовательского фонда (*англ*. National Research Foundation — NRF) (проект № 120456) в рамках научного проекта № 19-55-80010 и гранта CSC (*англ*. China Scholarship Council) № 202110280009.

Ключевые слова: RSEI, временные ряды, лесной покров, мониторинг, Landsat, Китай, анализ трендов, логистическая модель

Одобрена к печати: 20.10.2022
DOI: 10.21046/2070-7401-2022-19-5-176-189

Литература

1. *Badea O.*, *Apostol E.* Forest science innovation for sustainable forest management, improvement of human welfare, and quality of life under global environmental changes // Science of The Total Environment. 2020. V. 701. Art. No. 134429. 4 p. https://doi.org/10.1016/j.scitotenv.2019.134429.
2. *Chang X.*, *Zhao W.*, *Liu H.*, *Wei X.*, *Liu B.*, *He Z.* Qinghai spruce (*Picea crassifolia*) forest transpiration and canopy conductance in the upper Heihe River Basin of arid northwestern China // Agricultural and Forest Meteorology. 2014. V. 198–199. P. 209–220. http://dx.doi.org/10.1016/j.agrformet.2014.08.015.
3. *De Jong R.*, *Verbesselt J.*, *Schaepman M. E.*, *de Bruin S.* Trend changes in global greening and browning: contribution of short-term trends to longer-term change // Global Change Biology. 2012. V. 18. No. 2. P. 642–655. https://doi.org/10.1111/j.1365-2486.2011.02578.x.
4. *Eastman J. R.*, *Sangermano F.*, *Machado E. A.*, *Rogan J.*, *Anyamba A.* Global trends in seasonality of Normalized Difference Vegetation Index (NDVI), 1982–2011 // Remote Sensing. 2013. V. 5. No. 10. P. 4799–4818. https://doi.org/10.3390/rs5104799.
5. *Gao G.*, *Xin Z.*, *Ding G.*, *Li C.*, *Zhang J.*, *Linag W.*, *An Y.*, *He Y.*, *Xiao M.*, *Li W.* Forest health studies based on remote sensing: a review // Acta Ecologica Sinica. 2013. V. 33. No. 6. P. 1675–1689. https://doi.org/10.5846/stxb201112011838.
6. *Gorelick N.*, *Hancher M.*, *Dixon M.*, *Ilyushchenko S.*, *Thau D.*, *Moore R.* Google Earth Engine: Planetary-scale geospatial analysis for everyone // Remote Sensing of Environment. 2017. V. 202. P. 18–27. https://doi.org/10.1016/j.rse.2017.06.031.

7. *Jamali S.*, *Seaquist J.*, *Eklundh L.*, *Ardo J.* Automated mapping of vegetation trends with polynomials using NDVI imagery over the Sahel // Remote Sensing of Environment. 2014. V. 141. P. 79–89. https://doi.org/10.1016/j.rse.2013.10.019.
8. *Jin S.*, *Sader S.* Comparison of time series tasseled cap wetness and the normalized difference moisture index in detecting forest disturbances // Remote Sensing of Environment. 2005. V. 94. No. 3. P. 364–372. https://doi.org/10.1016/j.rse.2004.10.012.
9. *Kennedy R.*, *Cohen W.*, *Schroeder T.* Trajectory-based change detection for automated characterization of forest disturbance dynamics // Remote Sensing of Environment. 2007. V. 110. No. 3. P. 370–386. https://doi.org/10.1016/j.rse.2007.03.010.
10. *Kurbanov E.*, *Vorobiev O.*, *Gubayev A.*, *Moshkina L.*, *Leznin S.* Carbon sequestration after pine afforestation on marginal lands in the Povolgie region of Russia: A case study of the potential for a Joint Implementation activity // Scandinavian J. Forest Research. 2007. V. 22. No. 6. P. 488–499. https://doi.org/10.1080/02827580701803080.
11. *Kurbanov E.*, *Vorobiev O.*, *Sha J.*, *Li X.*, *Gitas I.*, *Minakou C.*, *Gabdelkhakov A.*, *Martynova M.* A survey on the use of GIS and remote sensing for sustainable forestry and ecology in Russia and China // Current Problems in Remote Sensing of the Earth from Space. 2020. V. 17. No. 5. P. 9–20. DOI: 10.21046/2070-7401-2020-17-5-9-20.
12. *Kurbanov E.*, *Vorobev O.*, *Lezhnin S.*, *Sha J.*, *Wang J.*, *Li X.*, *Cole J.*, *Dergunov D.*, *Wang Y.* Remote sensing of forest burnt area, burn severity, and post-fire recovery: a review // Remote Sensing. 2022. V. 14. No. 19. Art. No. 4714. 35 p. https://doi.org/10.3390/rs14194714.
13. *Lai S.*, *El-Adawy A.*, *Sha J.*, *Li X.*, *Wang J.*, *Kurbanov E.*, *Lin Q.* Towards an integrated systematic approach for ecological maintenance: case studies from China and Russia // Ecological Indicators. 2022. V. 140. Art. No. 108982. 19 p. https://doi.org/10.1016/j.ecolind.2022.108982.
14. *Lawrence R.*, *Ripple W.J.* Calculating Change Curves for Multitemporal Satellite Imagery Mount St. Helens 1980–1995 // Remote Sensing of Environment. 1999. V. 67. No. 3. P. 309–319. https://doi.org/10.1016/S0034-4257(98)00092-3.
15. *Mora F.* A suite of ecological indicators for evaluating the integrity of structural eco-complexity in Mexican forests // Ecological Complexity. 2022. V. 50. Art. No. 101001. 19 p. https://doi.org/10.1016/j.ecocom.2022.101001.
16. *Mu H.*, *Li X.*, *Ma H.*, *Du X.*, *Huang J.*, *Su W.*, *Yu Z.*, *Xu C.*, *Liu H.*, *Yin D.*, *Li B.* Evaluation of the policy-driven ecological network in the Three-North Shelterbelt region of China // Landscape and Urban Planning. 2022. V. 218. Art. No. 104305. 11 p. https://doi.org/10.1016/j.landurbplan.2021.104305.
17. *Peng H.*, *Cheng G.*, *Xu Z.*, *Yin Y.*, *Xu W.* Social, economic, and ecological impacts of the "Grain for Green" project in China: A preliminary case in Zhangye, Northwest China // J. Environmental Management. 2007. V. 85. No. 3. P. 774–784. https://doi.org/10.1016/j.jenvman.2006.09.015.
18. *Qiu B.*, *Chen G.*, *Tang Z.*, *Lu D. Wang Z.*, *Chen C.* Assessing the Three-North Shelter Forest Program in China by a novel framework for characterizing vegetation changes // *ISPRS* J. Photogrammetry and Remote Sensing. 2017. V. 133. P. 75–88. https://doi.org/10.1016/j.isprsjprs.2017.10.003.
19. *Riano D.*, *Chuvieco E.*, *Ustin S.*, *Zomer R.*, *Dennison P.*, *Roberts D.*, *Salas J.* Assessment of vegetation regeneration after fire through multitemporal analysis of AVIRIS images in the Santa Monica Mountains // Remote Sensing of Environment. 2002. V. 79. No. 1. P. 60–71. https://doi.org/10.1016/S0034-4257(01)00239-5.
20. *Tian A.*, *Wang Y.*, *Webb A.A.*, *Liu Z.*, *Ma J.*, *Yu P.*, *Wang X.* Water yield variation with elevation, tree age and density of larch plantation in the Liupan Mountains of the Loess Plateau and its forest management implications // Science of The Total Environment. 2021. V. 752. Art. No. 141752. 13 p. https://doi.org/10.1016/j.scitotenv.2020.141752.
21. *Verbesselt J.*, *Hyndman R.*, *Newnham G.*, *Culvenor D.* Detecting trend and seasonal changes in satellite image time series // Remote Sensing of Environment. 2010. V. 114. No. 1. P. 106–115. https://doi.org/10.1016/j.rse.2009.08.014.
22. *Wang C.*, *Wang A.*, *Guo D.*, *Li H.*, *Zang S.* Off-peak NDVI correction to reconstruct Landsat time series for post-fire recovery in high-latitude forests // Intern. J. Applied Earth Observation and Geoinformation. 2022. V. 107. Art. No. 102704. 14 p. https://doi.org/10.1016/j.jag.2022.102704.
23. *Wang J.*, *Xie Y.*, *Wang X.*, *Dong J.*, *Bie Q.* Detecting Patterns of Vegetation Gradual Changes (2001–2017) in Shiyang River Basin, Based on a Novel Framework // Remote Sensing. 2019. V. 11. No. 21. Art. No. 2475. 24 p. https://doi.org/10.3390/rs11212475.
24. *Wang Y.* Forest ecological monitoring of the Shiyang River basin based on Google Earth Engine // IOP Conf. Ser.: Earth and Environmental Science. 2021. V. 932. No. 1. Art. No. 012011. 9 p. https://doi.org/10.1088/1755-1315/932/1/012011.
25. *Wessels K.J.*, *van der Bergh F.*, *Scholes R.J.* Limits to detectability of land degradation by trend analysis of vegetation index data // Remote Sensing of Environment. 2012. V. 125. P. 10–22. https://doi.org/10.1016/j.rse.2012.06.022.

26. *Xiao Q.*, *Huang M.* Fine root distributions of shelterbelt trees and their water sources in an oasis of arid northwestern China // J. Arid Environments. 2016. V. 130. P. 30–39. https://doi.org/10.1016/j.jaridenv.2016.03.004.
27. *Xiong Y.*, *Xu W.*, *Lu N.*, *Huang S.*, *Wu C.*, *Wang L.*, *Dai F.*, *Kou W.* Assessment of spatial-temporal changes of ecological environment quality based on RSEI and GEE: A case study in Erhai Lake Basin, Yunnan province, China // Ecological Indicators. 2021. V. 125. Art. No. 107518. 10 p. https://doi.org/10.1016/j.ecolind.2021.107518.
28. *Xu H.*, *Wang M.*, *Shi T.*, *Guan H.*, *Fang C.*, *Lin Z.* Prediction of ecological effects of potential population and impervious surface increases using a remote sensing based ecological index (RSEI) // Ecological Indicators. 2018. V. 93. P. 730–740. https://doi.org/10.1016/j.ecolind.2018.05.055.
29. *Yang Y.*, *Monserud R.A.*, *Huang S.* An evaluation of diagnostic tests and their roles in validating forest biometric models // Canadian J. Forest Research. 2004. V. 34. No. 3. P. 619–629. https://doi.org/10.1139/x03-230.
30. *Yu J.*, *Li F.*, *Wang Y.*, *Lin Y. Peng Z.*, *Cheng K.* Spatiotemporal evolution of tropical forest degradation and its impact on ecological sensitivity: A case study in Jinghong, Xishuangbanna, China // Science of The Total Environment. 2020. V. 727. Art. No. 138678. 13 p. https://doi.org/10.1016/j.scitotenv.2020.138678.
31. *Yun Chen Y.*, *Wang J.*, *Kurbanov E.*, *Thomas A.*, *Sha J.*, *Jiao Y.*, *Zhou J.* Ecological security assessment at different spatial scales in central Yunnan Province, China // PLoS ONE. 2022. V. 17. No. 6. Art. No. e0270267. 19 p. https://doi.org/10.1371/journal.pone.0270267.
32. *Zhang X.*, *Friedl M.A.*, *Schaaf C.B.*, *Strahler A.H.*, *Hodges J.C.F.*, *Gao F.*, *Reed B.C.*, *Huete A.* Monitoring vegetation phenology using MODIS // Remote Sensing of Environment. 2003. V. 84. No. 3. P. 471–475. https://doi.org/10.1016/S0034-4257(02)00135-9.
33. *Zhang X.*, *Liu K.*, *Li X. Wang S.*, *Wang J.* Vulnerability assessment and its driving forces in terms of NDVI and GPP over the Loess Plateau, China // Physics and Chemistry of the Earth. 2022. V. 125. Art. No. 103106. 12 p. https://doi.org/10.1016/j.pce.2022.103106.
34. *Zhao J.*, *Ma J.*, *Zhu Y.* Evaluating impacts of climate change on net ecosystem productivity (NEP) of global different forest types based on an individual tree-based model FORCCHN and remote sensing // Global and Planetary Change. 2019. V. 182. Art. No. 103010. 10 p. https://doi.org/10.1016/j.gloplacha.2019.103010.